Journal of Nuclear Materials 463 (2015) 493–497

Contents lists available at ScienceDirect

Journal of Nuclear Materials

journal homepage: www.elsevier.com/locate/jnucmat

Intra-ELM phase modelling of a JET ITER-like wall H-mode discharge with EDGE2D-EIRENE

D.M. Harting [b,*,1], S. Wiesen [c], M. Groth [d], S. Brezinsek [c], G. Corrigan [b], G. Arnoux [b], P. Boerner [c], S. Devaux [b], J. Flanagan [b], A. Järvinen [d], S. Marsen [e], D. Reiter [c], JET-EFDA contributors [a,2]

[a] JET-EFDA, Culham Science Centre, Abingdon OX14 3DB, UK
[b] CCFE, Culham Science Centre, Abingdon, Oxon OX14 3DB, UK
[c] Institute of Energy and Climate Research – IEK4, Association EURATOM-FZJ, D-52425 Jülich, Germany
[d] Aalto University, Association EURATOM-Tekes, Espoo, Finland
[e] Max-Planck-Institut für Plasmaphysik, EURATOM-Association, D-17491 Greifswald, Germany

ARTICLE INFO

Article history:
Available online 13 December 2014

ABSTRACT

We present the application of an improved EDGE2D-EIRENE SOL transport model for the ELM phase utilizing kinetic correction of the sheath-heat-transmission coefficients and heat-flux-limiting factors used in fluid SOL modelling. With a statistical analysis over a range of similar type-I ELMy H-mode discharges performed at the end of the first JET ITER-like wall campaign, we achieved a fast (Δt = 200 μs) temporal evolution of the outer midplane n_e and T_e profiles and the target-heat and particle-flux profiles, which provides a good experimental data set to understand the characteristics of an ELM cycle. We will demonstrate that these kinetic corrections increase the simulated heat-flux-rise time at the target to experimentally observed times but the power-decay time at the target is still underestimated by the simulations. This longer decay times are potentially related to a change of the local recycling coefficient at the tungsten target plate directly after the heat pulse.

1. Introduction

Previous modelling of the full JET ELM cycle [1] in JET equipped with carbon walls (JET-C) has shown that the fluid approximation for the parallel transport in EDGE2D-EIRENE [2,3] is sufficient to reproduce the energy balance in terms of the ELM-wetted area and power in-out asymmetry. However, the peak-power load q_{max} obtained in the intra-ELM phase of those simulations was overestimated leading to an 8-times higher value of q_{max} compared to the experiment while the power-decay time at the target was underestimated. This resulted in a total (over time integrated) power load to the targets similar to those observed experimentally (and thus reproduced the characteristics of a free streaming approximation of ELM filamentary transport as proposed in Ref. [4]) but the time-wise evolution of q_{max} at the target still suffered from the assumption of the parallel scrape-off layer (SOL) transport being classical in the fluid simulations.

In fact, 1D kinetic simulation for a typical type-I ELMy JET SOL [5] have shown that within the intra-ELM phase, the fluid approximation for parallel transport in the SOL breaks down and kinetic effects play a significant role for the heat flux transported towards the target plate. It is specifically the electron-heat channel, which is strongly overestimated when using a classical fluid treatment for the parallel transport.

We present the results of the application of an improved EDGE2D-EIRENE SOL transport model for the intra-ELM phase of discharges from a two-week lasting JET ITER-like wall [6] (ILW) operation. A type-I ELMy H-mode neutral-beam heated tokamak discharge (I_p/B_t = 2.0 MA/2.0 T, P_{NBI} = 12 MW) in low triangularity had been continuously repeated to obtain a footprint of the material migration under quasi steady-state wall conditions prior to the removal of plasma-facing components for further analysis [7]. This group of discharges provides an unprecedented data set to statistically analyse the intra-ELM evolution of pedestal and target plasma profiles experimentally.

The derived time-dependent kinetic correction factors (KF) from [5], i.e. sheath-heat transmission-coefficients and kinetic heat-flux limiters are applied for simulations of the ELM phase of the aforementioned discharges. The sensitivity of the simulations on the kinetic effects is studied in order to match the experimentally

* Corresponding author.
E-mail address: Derek.Harting@ccfe.ac.uk (D.M. Harting).
[1] Presenting author.
[2] See the Appendix of F. Romanelli et al., Proceedings of the 24th IAEA Fusion Energy Conference 2012, San Diego, US.

http://dx.doi.org/10.1016/j.jnucmat.2014.12.023
0022-3115/

observed ELM peak power-loads and decay times derived from infrared thermography. The resulting more realistic ELM background plasma configurations (in the scope of 2D fluid SOL simulations) will be used further for material migration studies and tungsten source and transport analysis employing dedicated plasma-surface interaction codes such as WallDYN [8] and ERO [9].

2. Statistical ELM analysis

The previous modelling of the ELM crash [1] was compared to experimental data of discharge #73569 from JET-C. Later in Ref. [10] it was reported however that in JET-ILW the ELM duration can be much longer than in JET-C, but with increased pedestal temperature the ELM duration could be reduced in JET-ILW. ELMs with long duration are also present in the discharges we analyse here: Fig. 1 shows the pedestal drop after the ELM crash (determined from D_α and WI radiation at the inner target) for the previously modelled discharge #73569 from JET-C and one of the ILW discharges analysed in this paper. The time resolution of the edge interferometer channel for the density measurement has significantly improved after the JET-C campaigns, which allows the estimation of the density pedestal drop time only for the JET-ILW discharge #83559. The fast drop in edge electron temperature measured by the edge ECE channel and in the stored energy measurement indicates ELM durations for JET-C (#73569) below the temporal resolution of the measurement (<400 μs). For the ILW discharge, the drop of the pedestal density and temperature extends over a much longer range of 4–5 ms after the ELM crash, which was not anticipated before the installation of the JET-ILW.

2.1. Outer midplane plasma profiles

The high resolution Thomson scattering (HRTS) diagnostic at the outer midplane (OMP) of JET can measure every 50 ms radial n_e and T_e profiles. This frequency is much too slow to resolve the evolution of the density and temperature pedestal during an ELM. To obtain an evolution of n_e and T_e profiles with a time resolution of $\Delta t = 200$ μs, we extracted the HRTS measurements relative to the ELM crash, for which we used the integrated inner target WI-emission from physical sputtering as an indicator. For the statistical analysis we used 53 similar discharges from the range #83628–#83727 and averaged 20–50 individual HRTS

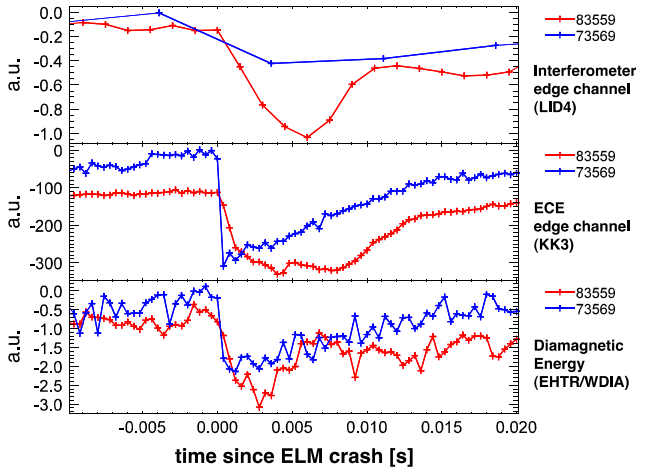

Fig. 1. Drop of the pedestal density (top graph), electron temperature (middle graph) and stored energy (bottom graph) after the ELM crash for the previously modelled JET-C pulse #73569 (blue curves) and the JET-ILW pulse #83559 (red curves). (For interpretation of the references to colour in this figure legend, the reader is referred to the web version of this article.)

measurements in a time window of $\Delta t = 200$ μs (averaging out also any filamentary structures). We restricted the statistical analysis to times between 10.0 s and 14.0 s of the discharge with an average ELM frequency of $f_{ELM} \approx 30$ Hz. In our statistical analysis only ELMs which had an ELM-free time of $\Delta t = 20$ ms before and after the ELM were taken into account. The profiles from the statistical analysis of the HRTS measurements for dedicated times points after the ELM trigger ($t = 0$ corresponds to the last OMP profile, unaffected by the ELM) are shown in Fig. 2, defining different phases of the time evolution of the OMP profiles.

Electron density profile evolution at the OMP:

Phase 1: The electron density at the top of the pedestal drops quickly in the first 0.4 ms after the ELM crash (green curve) by 25%. In this first 0.4 ms the particles are flushed into the SOL, where the density increases from $1 \times 10^{19}\,m^{-3}$ to $\sim 2.5 \times 10^{19}\,m^{-3}$.
Phase 2: From 0.4 ms to ~1.6 ms (blue curve) the density stays about constant in the SOL, but is still dropping slightly up to 10 cm inside the separatrix.
Phase 3: Due to a reduced fuelling of the pedestal, the density drops after 1.6 ms further in the SOL up to 2.5 cm inside the separatrix to its lowest profile around ~5.2 ms (pink).
Phase 4: After 5.2 ms, the density recovers to its initial pre-ELM profile until the next ELM is triggered.

Electron temperature profile evolution at the OMP:

Phase 1: In the first 0.4 ms some of the pedestal heat is flushed into the SOL.
Phase 2: After 0.4 ms the electron temperature drops steady going until ~1.2 ms to its lowest profile (blue).
Phase 3: From 1.2 ms to ~2.8 ms the electron temperature stays then roughly constant.
Phase 4: After 2.8 ms the electron temperature pedestal starts recovering.

This behaviour can also be observed in the evolution of the relative pedestal density and temperature drops ($\Delta n_e/n_e$, $\Delta T_e/T_e$) shown in Fig. 3.

2.2. Outer target heat and particle flux profiles

Due to a high time resolution of the measurements for the heat flux by the infrared camera (IR) and the particle flux measured by Langmuir probes at the outer target (OT) we only needed to extract and average profiles relative to the ELM crash in the statistical analysis from one discharge (#83562) to achieve a sufficient number of individual measurements in each time window (Fig. 4). The heat flux at the outer target peaks quickly at 0.6 ms before it slowly decays until ~5 ms. The particle flux starts rising at the same time as the heat flux but has a delayed peak at ~1.2 ms before it decays slowly until ~5–6 ms. A strong second peak in the particle flux can be observed around 8 ms. The origin of this second peak in the particle flux is currently not clear.

3. Simulation of the intra-ELM phase

In order to simulate the intra-ELM phase with the EDGE2D-EIRENE code, we first simulated pure deuterium (no impurities) steady-state pre-ELM conditions. We used 10.5 MW (12 MW NBI heating, 0.5 MW ohmic heating, −2 MW core radiation) of input power entering the simulation domain from the core (uniformly distributed between electrons and ions) and setup a transport barrier by dropping the anomalous perpendicular transport

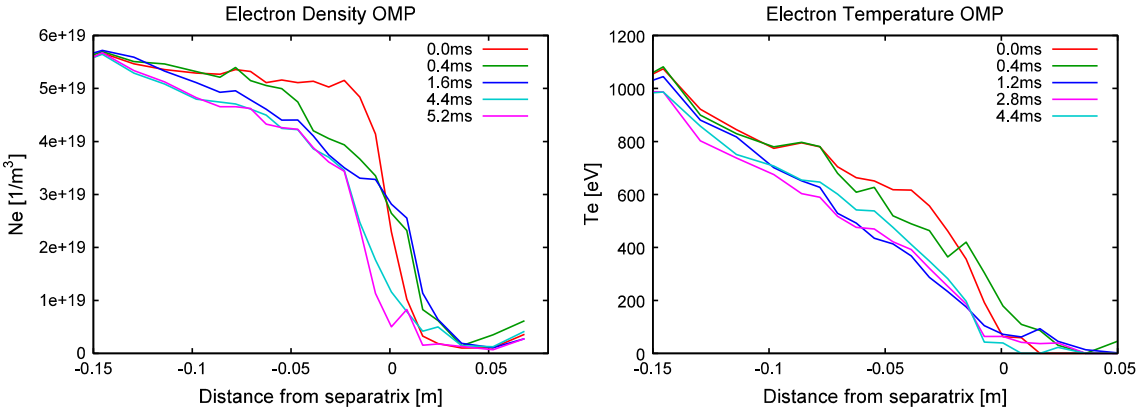

Fig. 2. Averaged OMP electron density and temperature profiles from the statistical analysis of the HRTS data for characteristic time points after the ELM crash.

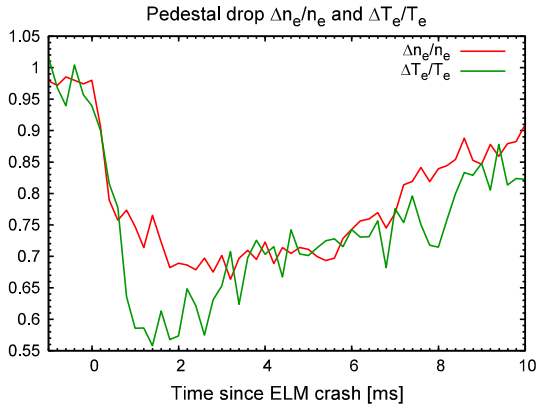

Fig. 3. Temporal evolution of the relative pedestal drops at the OMP of the averaged electron density (2.5 cm inside separatrix) and temperature (3.3 cm inside separatrix) from the statistical analysis of the HRTS data.

coefficients in the first few centimetres inside the separatrix to $\chi_e = \chi_i = 0.5\ m^2\ s^{-1}$ for the electron and ion perpendicular heat conductivity and to $D = 0.04\ m^2\ s^{-1}$ for the perpendicular particle diffusivity. The transport barrier for the particles is also extended 1.5 cm into the SOL, to match the experimental pre-ELM OMP density profiles. The OMP separatrix density $n_{sep,OMP} = 2.4 \times 10^{19}\ m^{-3}$ is achieved by a fixed injection rate and we used default heat-flux limiting factors [11] for electrons and ions of $\alpha_{0e} = \alpha_{0i} = 0.2$. The sheath heat transmission factors were set in the pre-ELM phase to $\gamma_e = 2.5$ and $\gamma_i = 4.5$ for electrons and ions respectively.

The 1D kinetic modelling in Ref. [5] has shown that during transient processes such as ELM's the boundary conditions for the ion parallel speed and particle energy fluxes at the sheath entrance as well as the parallel heat fluxes are strongly dominated by kinetic effects. They derived kinetic correction factors (KF) in order to allow for a simplified treatment of these kinetic effects in codes using the fluid approximation. We implemented now the kinetic corrections factors proposed in Ref. [5] by using the formulas for

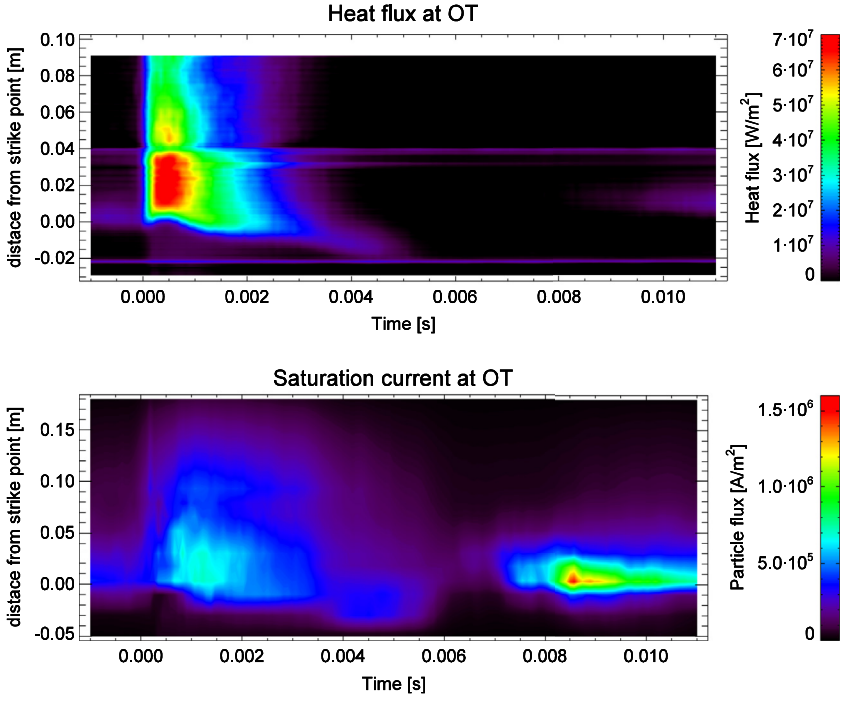

Fig. 4. Averaged heat and ion saturation current profiles at the OT from the statistical analysis.

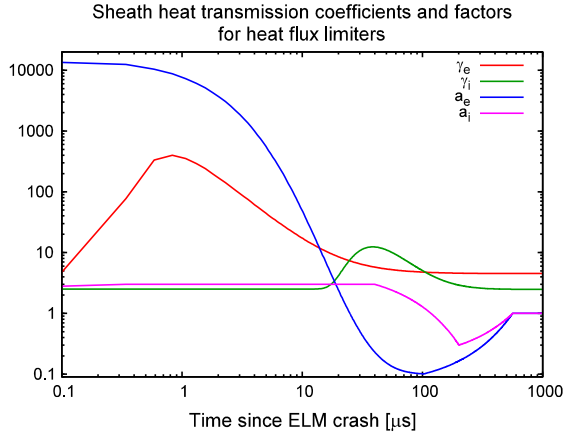

Fig. 5. Sheath heat transmission coefficients γ_i, γ_e and heat flux limiting factors a_i, a_e normalized to pre ELM values α_{0e}, α_{0i}.

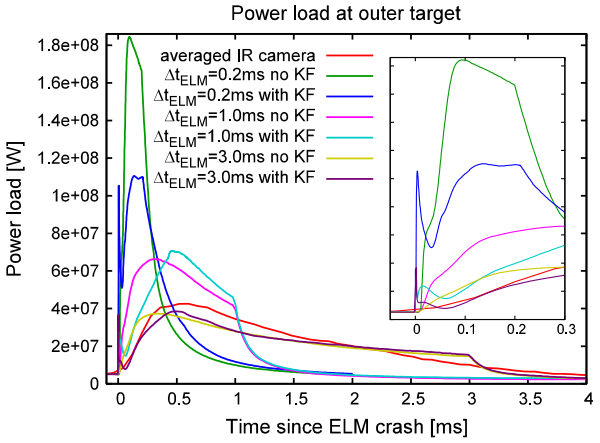

Fig. 6. Comparison of the temporal evolution of the integrated power load on the OT between IR measurement and different ELM durations in the simulations. The second graph inside the first one is a zoom into the region between $t = -0.05$ ms and 0.3 ms to illustrate the pre peak in heat flux originated from the KF.

the sheath-heat-transmission factors described in the paper. For the electron and ion heat-flux limiting factors we applied the following parameterization normalized to the pre-ELM heat-flux limiting factors α_{0e}, α_{0i} as a simplified fit to the KF shown in Ref. [5] (with t in μs):

$$a_e(t) = \begin{cases} 0.1e^{(12e^{(-t/15)})} & \text{for } 0 < t < 100 \\ 0.1e^{((t-100)/200)} & \text{for } 100 < t < 560 \\ 1 & \text{else where} \end{cases} \quad (1)$$

$$a_i(t) = \begin{cases} 3 & \text{for } 0 < t < 40 \\ 3e^{(-(t-40)/70)} & \text{for } 40 < t < 200 \\ 0.3e^{((t-200)/300)} & \text{for } 200 < t < 560 \\ 1 & \text{else where} \end{cases} \quad (2)$$

The implemented KF are shown in Fig. 5 where the heat-flux-limiting factors were normalized to its pre-ELM values α_{0e} and α_{0i}.

Similar to Ref. [1] the ELM model in EDGE2D-EIRENE allows specifying a radial profile of modified perpendicular transport coefficient for a selected duration Δt_{ELM} of the ELM. Here we chose a triangular spatial shape peaking at or slightly inside the separatrix with a radial extend at the OMP of 7 cm inside the separatrix and 1 cm outside into the SOL. Beyond this region, the perpendicular diffusivities and conductivities were set to 1 $m^2\,s^{-1}$. We investigated three different ELM durations of $\Delta t_{ELM} = 200$ μs, 1 ms and 3 ms. The corresponding peak transport coefficients of the spatial triangular shape are listed in Table 1 together with the achieved ELM energies ΔE_{ELM}. The first line of Table 1 lists the corresponding experimental values. The experimental ELM energy was estimated here in two ways. With the assumption of $T_i = T_e$ we calculated from the averaged experimental OMP n_e and T_e profiles the stored energy and estimated an ELM energy of 120 kJ. By applying the same statistical analysis as described above for the measured diamagnetic energy W_{DIA}, we estimated an average ELM energy of 160 kJ, which suggest an experimental ELM energy in the range of 120–160 kJ.

By applying a very short ELM duration of $\Delta t_{ELM} = 200$ μs (as used in previous ELM simulations [1]) we underestimate the pedestal drop times at the OMP for the electron density ($t_{drop,ne}$) and temperature ($t_{drop,Te}$) as well as the rise ($t_{peak,Q}$) and the decay ($t_{decay,Q}$) times of the heat flux at the OT dramatically (see Table 1). By applying the kinetic correction factors (KF) proposed in Ref. [5], we can increase the rise and decay times of the heat flux at the OT by 0.1 ms, but this is still not enough to get to the experimental raise time of 1.2 ms. Also the peak-power load is reduced nearly by a factor of two, while applying the KF (Fig. 6). The spreading of the heat load over a larger time window is mainly attributed to the strong limitation of the electron heat flux. The additional pre-peak observed in the heat load at 4 μs while applying the KF is a combination effect of the reduced electron heat flux limit and the strongly increased electron sheath heat transmission factor at that time.

By increasing the ELM duration to $\Delta t_{ELM} = 1$ ms, we can achieve an electron temperature pedestal drop time similar to the experimental drop time of 1 ms but a slightly too long density pedestal drop time of 0.75 ms. Also the raise and decay times of the heat flux are still too short. By applying the KF to the 1 ms ELM duration simulation, we can nearly achieve the experimental density pedestal drop time and OT heat flux rise time. The heat-flux decay time at the OT is unaffected by the KF.

If we further increase the ELM duration to $\Delta t_{ELM} = 3$ ms, we can match the decay time of the heat flux, but the pedestal drop times

Table 1
Overview of the experimental and simulated ELM parameters including ELM energy ΔE_{ELM}, peak value of perpendicular transport coefficients during the ELM, the pedestal drop times of n_e ($t_{drop,ne}$) and T_e ($t_{drop,Te}$), and the raise ($t_{peak,Q}$) and decay ($t_{decay,Q}$) times of the heat flux at the outer target.

Case	ΔE_{ELM} (kJ)	D_{ELM} (m^2/s)	$\chi_{e,ELM}$ (m^2/s)	$\chi_{i,ELM}$ (m^2/s)	$t_{drop,Te}$ (ms)	$t_{drop,ne}$ (ms)	$t_{peak,Q}$ (ms)	$t_{decay,Q}$ (ms)
Exp.	120–160	–	–	–	1.2	0.4	0.56	4
$\Delta t_{ELM} = 0.2$ ms no KF	97	200	100	300	0.2	0.2	0.09	0.64
$\Delta t_{ELM} = 0.2$ ms with KF	92	200	100	300	0.2	0.2	0.14	0.76
$\Delta t_{ELM} = 1.0$ ms no KF	125	10	30	30	1.0	0.75	0.3	1.53
$\Delta t_{ELM} = 1.0$ ms with KF	124	10	30	30	1.0	0.5	0.46	1.53
$\Delta t_{ELM} = 3.0$ ms no KF	156	10	6	6	3.0	2.2	0.35	3.65
$\Delta t_{ELM} = 3.0$ ms with KF	155	10	6	6	3.0	2.2	0.5	3.65

are much too long compared to the experimental pedestal drop times. Also in this case, if we apply the KF, we can increase the heat flux raise time from 0.35 ms to 0.5 ms, which is very close to the experimentally observed 0.56 ms.

4. Discussion and conclusion

From the experimental OMP electron density and temperature profiles in Fig. 2 we can conclude, that we have a short (400 μs) ELM event (MHD), which drops the pedestal density by 25%, destroys the transport barrier and flushes particles and heat into the SOL. The electron temperature profiles continue then to drop steady going until 1.2 ms while the density profile stays roughly constant until 1.6 ms (with a slight decrease in the first 10 cm inside the separatrix). After 1.6 ms the fuelling of the plasma is reduced until ≈5.2 ms, which reduces the SOL density up to 2.5 cm inside the separatrix. The reduced fuelling of the plasma between 1.6 ms and 5.2 ms must be associated with a transient particle pump during this period. As the fuelling of the plasma is determined by the recycling at the target plates and not the deuterium injection, it is likely that temporary the recycling coefficient at the target plate is reduced representing a sink for the plasma. The temperature profile on the other hand stays roughly constant between 1.2 ms and 2.8 ms and starts recovering at 3–4 ms, which suggests that the transport barrier re-establishes around that time.

The simple ELM model available in EDGE2D-EIRENE cannot reproduce this complex behaviour during the ELM cycle at the moment. But we could demonstrate that the inclusion of kinetic corrections to the heat flux limits (proposed in Ref. [5]) can reproduce the pedestal drop times $t_{drop,Te}$ and $t_{drop,ne}$, as well as the rise time $t_{peak,Q}$ of the heat flux at the outer target. We suggest extending the current ELM model in EDGE2D-EIRENE by a second phase (after the first 400 μs) where no transport barrier is applied and an additional particle pump at the target plate would account for the reduced pedestal fuelling before the transport barrier (around 3–4 ms) has been re-established. This could potentially reproduce the long decay times of the heat flux observed experimentally together with the fast drop (400 μs) of the density pedestal.

Acknowledgments

This project has received funding from the European Union's Horizon 2020 research and innovation programme under grant agreement number 633053 and from the RCUK Energy Programme [grant number EP/I501045]. The views and opinions expressed herein do not necessarily reflect those of the European Commission.

References

[1] S. Wiesen et al., Plasma Phys. Control. Fusion 53 (2011) 124039.
[2] R. Simonini, G. Corrigan, et al., Contrib. Plasma Phys. 34 (1994) 368–373.
[3] S. Wiesen, <http://www.eirene.de/e2deir_report_30jun06.pdf>.
[4] W. Fundamenski, R.A. Pitts, et al., Plasma Phys. Control. Fusion 48 (109) (2006).
[5] D. Tskhakaya et al., Contrib. Plasma Phys. 48 (1–3) (2008) 89–93.
[6] G.F. Matthews et al., Phys. Scr. 2011 (2011) 014001.
[7] S. Brezinsek et al., Nucl. Fusion 53 (2013) 083023.
[8] K. Schmid et al., J. Nucl. Mater. 415 (2011) 284.
[9] A. Kirschner et al., Nucl. Fusion 40 (5) (2000) 989.
[10] B. Sieglin et al., Plasma Phys. Control. Fusion 55 (2013) 124039.
[11] P.C. Stangeby, The Plasma Boundary of Magnetic Fusion Devices, IOP Publishing Ltd, Bristol UK, 2000.